Electronic Supplementary Material (ESI) for Journal of Materials Chemistry C.
This journal is © The Royal Society of Chemistry 2017

Supporting information

Design of UV-Crosslinked Polymeric Thin Layers for Encapsulation of Piezoelectric ZnO Nanowires for Pressure-Based Fingerprint Sensors

Agathe Bouvet-Marchand,[a,h] Alain Graillot,[a*] János Volk,[b] Rolanas Dauksevicius,[c] Chris Sturm,[d] Marius Grundmann,[d] Elise Saoutieff,[e] Antoine Viana,[e] Björn Christian,[f] Vadim Lebedev,[f] János Radó,[b,g] István E. Lukács,[b,g] Nguyen Quoc Khánh,[b] David Grosso,[h] Cedric Loubat[a]

[a] SPECIFIC POLYMERS, 34160 Castries, France
[b] MTA EK Institute of Technical Physics and Materials Science, 1121 Budapest, Hungary
[c] Kaunas University of Technology, Institute of Mechatronics, 51424 Kaunas, Lithuania
[d] Universität Leipzig, Institut für Experimentelle Physik II, 04103 Leipzig, Germany
[e] Université Grenoble Alpes, CEA, LETI, MINATEC Campus, F-38054 Grenoble, France
[f] Fraunhofer Institut fur Angewandte Festkorperphysik, 79108 Freiburg, Germany
[g] Óbuda University, Doctoral School on Material Sciences and technologies, 1034 Budapest, Hungary
[h] Université Aix-Marseille, IM2NP, 13397 Marseille, France

Contents

S 1. Photograph of the fingerprint sensor

S 2. Spin-coating deposition process

S 2.1 Theoretical relation between thickness and rotation speed

S 2.2 Thickness measurements

S 2.2.1 Optical methods

S 2.2.2 Correlation between optical methods and SEM

S 3. Consolidation of the as-grown NWs

S 4. Chemical inertness

S 1. Photograph of the fingerprint sensor

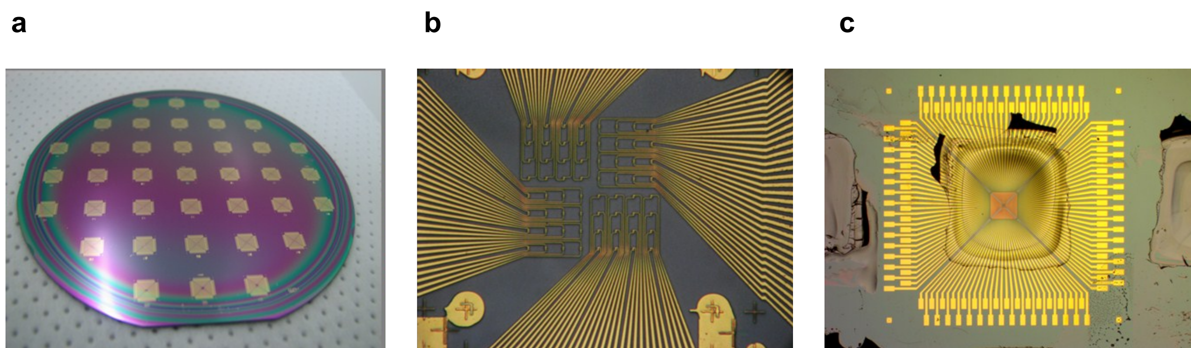

Figure S1. (a) Processed " Si wafer with 37 patterned chips (b) optical microscopy image of the centre of the chip before NW growth (c) chip encapsulated with polymer formulation

S 2. Spin-coating deposition process

S 2.1 Theoretical relation between thickness and rotation speed

Theoretical studies on the relation between film thicknesses and deposition process parameters were performed by Emslie et al. for a fluid where solvent evaporation did not occur.[1] It was found that film thickness (h) was proportional to some power of the fluid viscosity (μ), the angular velocity (ω) and the rotation time (t) according to the following equation:

$$\mathrm{h} = K.\mu^{1/2}.t^{-1/2}.\omega^{-1}$$

In Figure S1, experimental thickness measurements of the formulations with different HdA/PPGdA ratios are plotted as a function of the spin-coating rotation speed and compared to the theoretical curve derived from the equation above. K is arbitrary fixed at 5300 in order to compare these two curves in the same thickness range. It can be observed that experimental and theoretical curves follow the same trend, which demonstrate that the systems developed in this study can be properly described by this model.

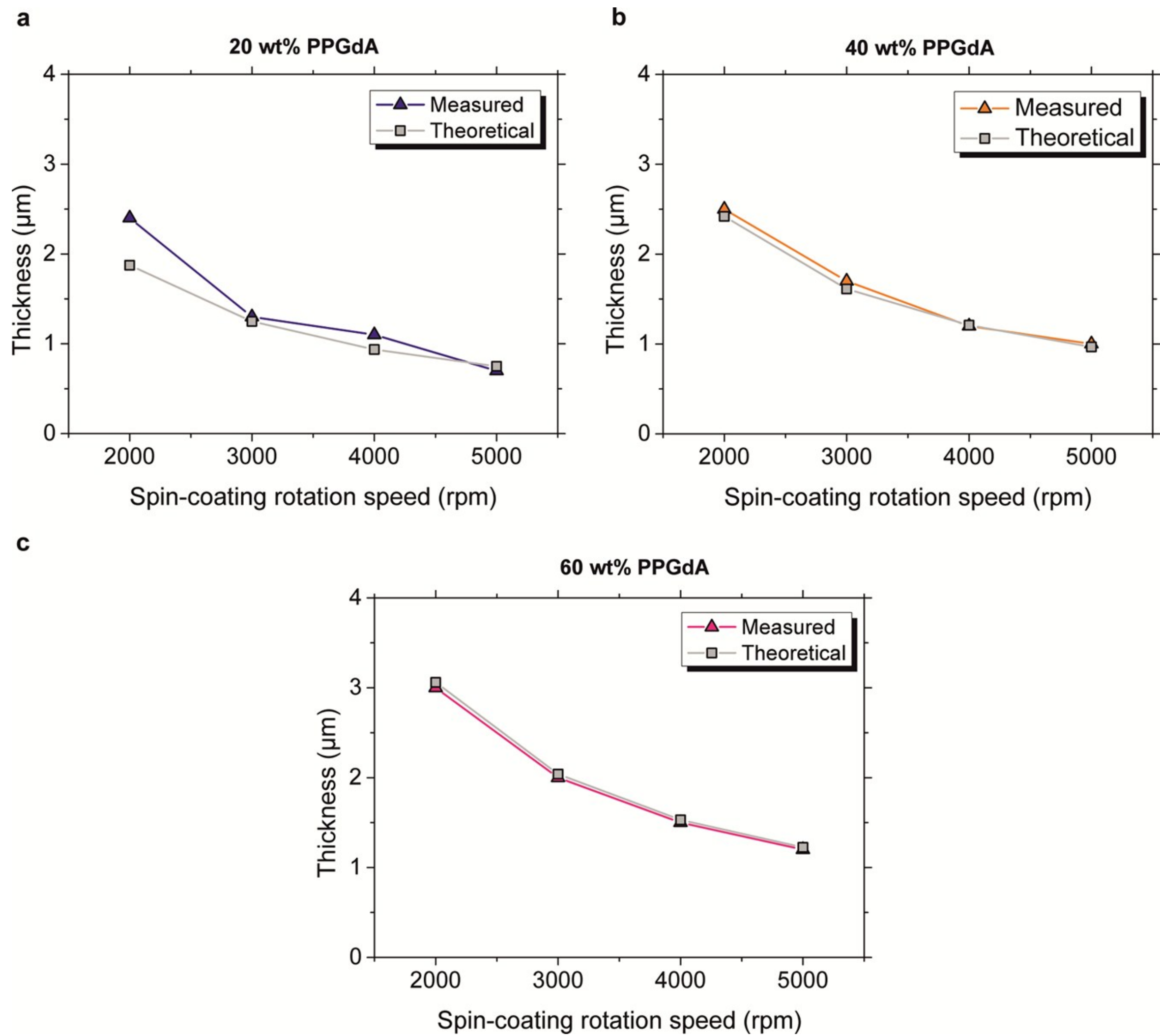

Figure S2. Representation of the experimental and theoretical film thicknesses as a function of the rotation speed during spin-coating for the three encapsulating layer formulations: (a) 80 HdA/20 PPGdA (b) 60 HdA/40 PPGdA(c) 40 HdA/60 PPGdA.

S 2.2 Thickness measurement methods

S 2.2.1 Optical methods

As explained in more detail in the manuscript, the polymer cap height (h_{pol}) has an important impact on the performance of the fingerprint sensor since it strongly influences the magnitude of the generated piezoelectric signals. A calibration curve of the deposited thickness as a function of the rotation speed was established to know how to adjust the spin-coating process in order to reach the targeted polymer cap height. The implementation of this calibration curve supposed to be able to accurately measure the thin layer thicknesses and, in particular, in the vicinity of the NW array.

To achieve this aim, a confocal spatially resolved micro-reflection was used with a Xenon lamp as light source. Since the spot on these experiments had a diameter of about 2-5 µm, the patterning of the sample by the metal contact lines could be neglected and the thickness of the polymer could be investigated. Then, the measured reflectivity spectra were described by a layer stack model taking into account the refractive index as well as the thickness of each layer. However, the drawback of this method is that it measures only the absolute reflectivity values and phase changes of the reflected light cannot be determined. A simplified structure using a 3-layer stack model was thus used to reduce the correlation between the thickness and the refractive index of each layer. This

model consisted of a Si substrate covered by a SiO_2 layer and the polymer encapsulation layer as a top layer. The optical properties of the Si and SiO_2 layer were taken from the literature and those of the polymer layer were determined in a previous experiment by spectroscopic ellipsometry.[2] The Cauchy parameters $A = 1.496$ and $B = 5 \times 10^{-3} \mu\mathrm{m}^2$ of the polymer layer were deduced from the spectrum presented in Figure S2 conducting to the calculation of the refractive index according to the Cauchy's equation : $n = A + \frac{B}{\lambda^2}$ (with λ the wavelength). The thickness of the SiO_2 layer was also fixed to 900 nm (layer deposited during the chip fabrication) to avoid correlation with the polymer thickness. The thickness of the polymer layer was then obtained by the best match between the calculated and experimental spectra.

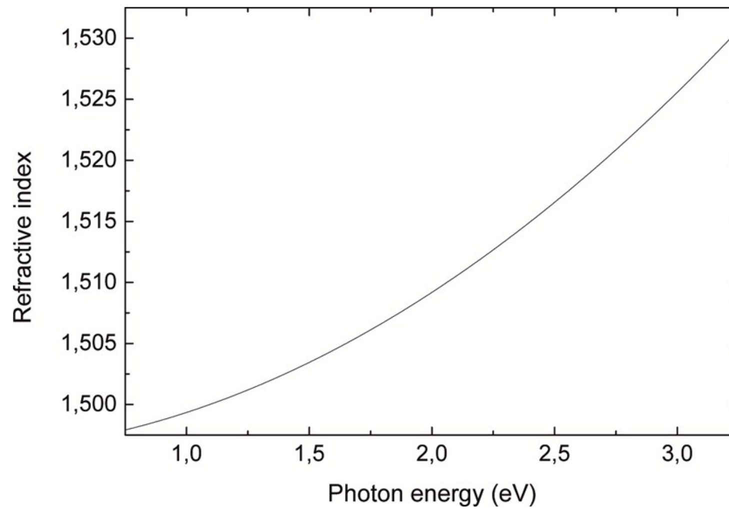

Figure S3. The determined refractive index of the encapsulating polymer as a function of the energy.

In parallel to this first method, spectroscopic ellipsometry was also performed on the encapsulating layer deposited on the electronic chip. Contrary to the micro-reflectance where the thickness is measured very locally, ellipsometry measures the average thickness over the whole sample. The ellipsometry principle relies on the determination of the change of a polarized light beam after reflection on the sample. Ellipsometry measures the complex reflectance ratio ρ which is the ratio of Fresnel reflection coefficients r_p over r_s, for light polarizations parallel and perpendicular to the plane of incidence respectively. The hereby defined reflection coefficients determine the ellipsometric angles ψ and Δ, as expressed in the equation below.

$$\rho = \frac{r_p}{r_s} = \tan \Psi e^{i\Delta},$$

Similar to the micro-reflectance spectrum, the recorded spectra was analyzed by using a five-layer stack model consisting of a Si substrate/SiO_2/W/SiO_2/polymer layer. The patterning of the tungsten layer was described by an effective medium approximation which averaged the optical properties of tungsten and SiO_2.

Due to the spin-coating technique, the thickness of the deposited polymer layer slightly differed locally. The probed area (200 µm × 500 µm) was much larger than the local change of the polymer thickness and thus the recorded spectrum was an average taken over microscopically different polymer thicknesses. For the analysis of the spectra, this effect was described by a thickness inhomogeneity in the layer stack model. In order to reduce the correlation between the thickness and the refractive index of the polymer layer, samples with different thicknesses ranging from 320 nm up to 2.6 µm were investigated and analyzed simultaneously, i.e. assuming that they differ only in the polymer thickness and thickness inhomogeneity. For example, Figure S3 shows the recorded spectra for a sample with a polymer layer thickness of about 320 nm.

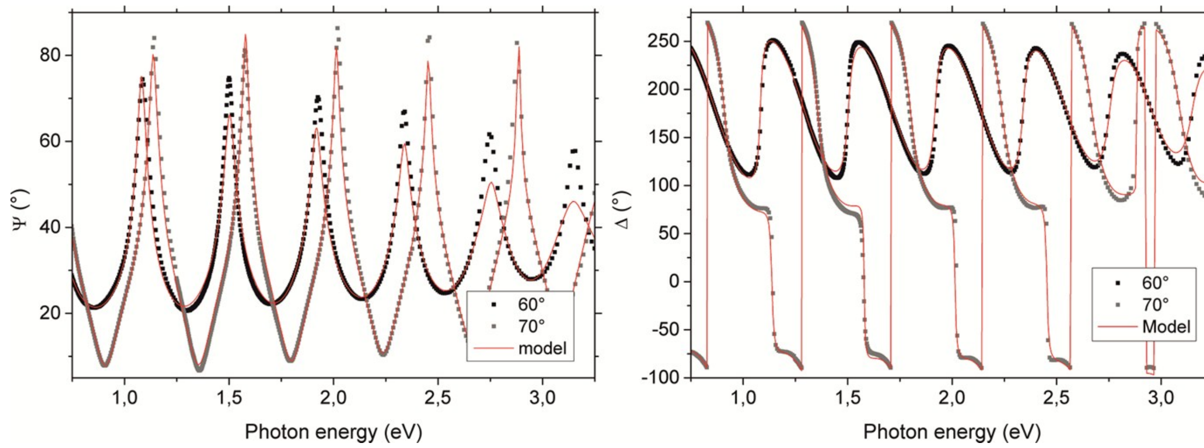

Figure S4. Experimental (symbols) and calculated (lines) spectra for a sample with a 320-nm-thick polymer layer for an angle of incidence of 60° (black symbols) and 70° (gray symbols).

The superposition of the calculated and experimental curves indicates a good agreement between the model and the measurements.

S 2.2.2 Correlation between optical methods and SEM

In addition to the aforementioned optical methods, SEM measurements were also carried out to determine the polymer encapsulation layer thicknesses. In Figure S4, it can be observed that polymer thicknesses measured by SEM are much lower than the ones measured by ellipsometry and micro-reflectance, although the images were taken from the same spatial position. Indeed, except for the highest rotation speed at 8000 rpm, the thicknesses differ by a factor of 2. The inconsistency between optical measurements (ellipsometry and micro-reflection) and SEM cannot be explained by (i) uncertainties of the SiO_2 thicknesses as the values are comparable in both optical and SEM samples, (ii) uncertainty of the used refractive index of the polymer since this would require a refractive index of about 2.3 instead of 1.51, determined previously on a reference sample and (iii) the beats coming from a high contrast between the refractive index of the SiO_2 and the polymer layer as they were not observable in the recorded spectra.

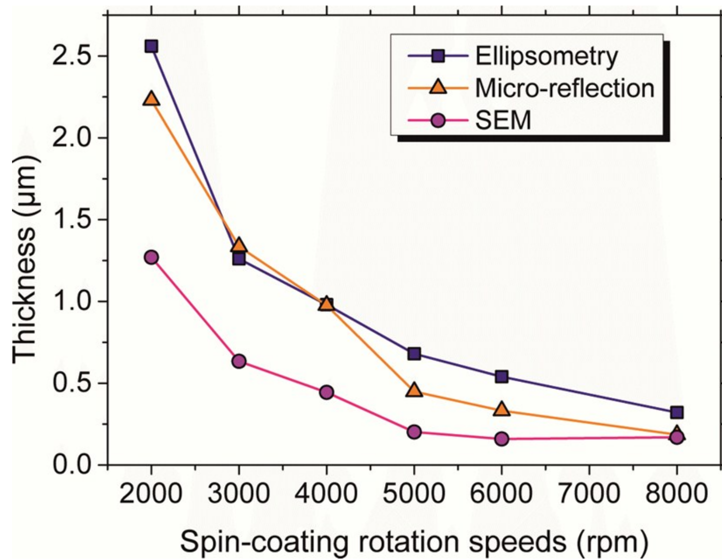

Figure S5. Encapsulation layer thickness as a function of the spin-coating rotation speed. Thickness was measured by means of three different methods: ellipsometry, micro-reflectance and SEM.

Therefore, further investigations were performed by laser microscopy in the vicinity of the NW array to measure the height profile. It can be observed on Figure S5 that the height in the regions investigated by SEM, ie. the regions between the NWs, was systematically reduced.

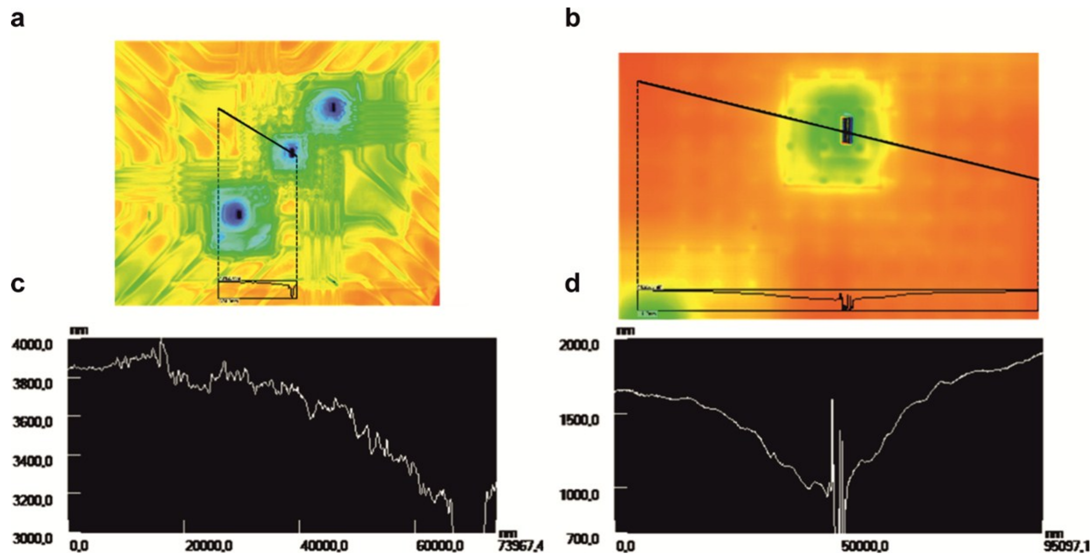

Figure S6. Height profile in the region of the ZnO seed layer spots (a) and in the region in between the NWs (b). Height profile (c,d) for the region marked by the black line respectively in (a) and (b).

The height differences between the sample surface and the investigated areas by SEM, are presented for each spin-coating rotation speeds in Figure S6a. It can be seen that the surface height difference is increasing with an increase of the polymer thickness. In Figure S6b, the difference of the polymer layer thicknesses determined by SEM and micro-reflectance, is given for each spin-coating rotation speeds.

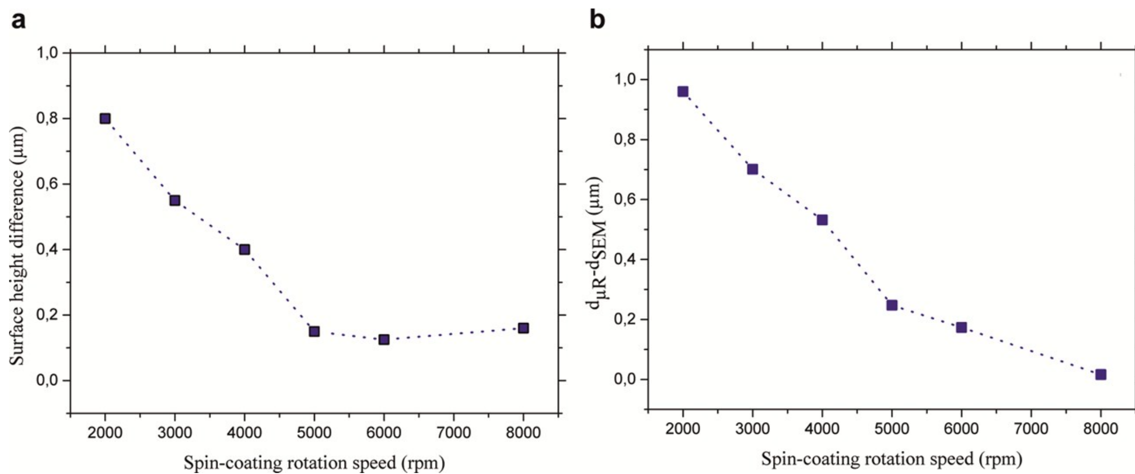

Figure S7. (a) The determined difference of the surface height by using a laser microscope on SEM-measured samples as a function of the spin-coating rotating speed (b) Difference between the polymer layer thicknesses determined by SEM and by micro-reflectance as a function of the spin-coating rotation speed.

By comparing these two graphs, it can be highlighted that the difference between the thicknesses measured by SEM and by micro-reflectance are in the same range as the surface height difference observed on the SEM samples. Thereby, it was concluded that the inconsistency of values between the optical and SEM methods was caused by a modification of the polymer layer during the microscopic measurements, certainly caused by the electron beam irradiation. Further studies are underway to explain the polymer collapsing, using nano-indentation technology. Based on this observation, the next investigations on the polymer layer thickness were performed with optical methods.

S 3. Consolidation of the as-grown NWs

Mechanical stress measurements were performed by SEM micromanipulator on the as-grown NWs. The results indicated that the mechanical strength was quite low (Figure S7a). The bare NWs were not able to withstand the constraint of the SEM micromanipulator tip and broke at their root (Figure S7b).

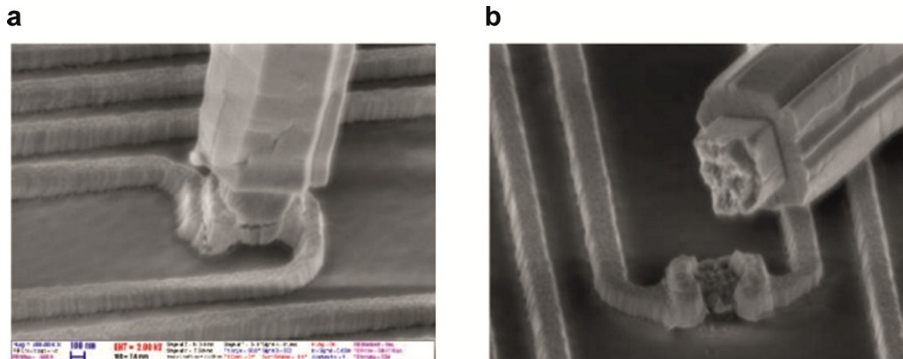

Figure S8. SEM image of a NW undergoing mechanical stress measurements upon SEM micromanipulator bending, leading to the formation of cracks at the NW root (left) followed by a complete fracture of the NW (right).

Further experiments demonstrated that the cracks of the NWs were induced by the fragility due to the reduced cross-section at the interface of the ZnO island and the NW, exhibiting a lot of cracks and/or void rich regions. NW's robustness was then enhanced by modifying the growth conditions.

S 4. Chemical inertness

Since the encapsulating layer corresponds to the part of the sensor that is in direct contact with the environment, it must also exhibit other specific properties such as hydrophobicity, oleophobicity and chemical inertness. The resistance to solvent was evaluated here on the developed encapsulating layer. The selected formulation (40 wt% of PPGdA and 60 wt% of HdA) was poured into silicon mould and UV-cured for 120 seconds. The sample was cut in two and one of the pieces was immersed in acetone for 1h. The other piece was used as a reference. After immersion, the sample was then dried in the open air for 24h.

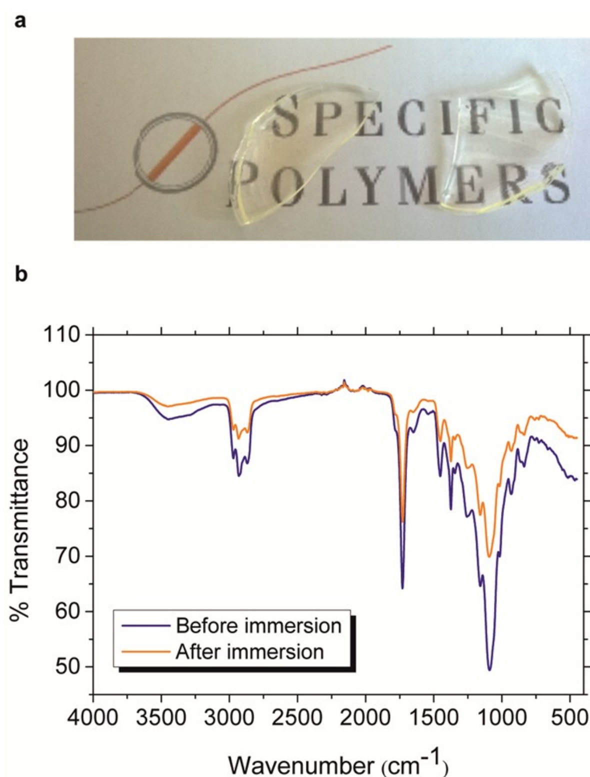

Figure S9. Solvent resistance of the encapsulating layer (a) Photograph of two pieces of the material: non-immersed sample (left) and immersed sample (right) (b) FTIR of the non-immersed and immersed sample.

The dried sample remained transparent after the process, did not whiten and was thereby similar to the non-immersed sample (Figure S8a). A gravimetric analysis was also performed on the sample before and after immersion. The proportion of insoluble polymer was equal to 100% which demonstrated that the material was not degraded by the solvent. Besides, Fourier Transform Infrared spectroscopy (FTIR) measurements were also carried out on the sample before and after immersion. All the characteristic peaks of the resin remained unchanged after immersion (Figure S8b), which confirmed that the material resisted to the solvent and no chemical reactions occurred.

References

1. Emslie, A. G.; Bonner, F. T.; Peck, L. G. Flow of a Viscous Liquid on a Rotating Disk. J Appl Phys. 1958,29, 858-862.
2. Palik, E. D.; Ghosh, G., Handbook of optical constants of solids. Academic Press: San Diego, 1998.